Acousto-optical coupling in two-dimensional air-slot phoxonic crystal heterostructure cavity

Ma Zhen-Meng[1], Tian Miao[1,*], Zhang Lei[1], Gao Pei-Feng[2]

[1] School of Mathematics and Physics, Lanzhou Jiaotong University,
 Lanzhou 730070, China

[2] Key Laboratory of Mechanics on Western Disaster and Environment of Ministry of Education,
 College of Civil Engineering and Mechanics,
 Lanzhou University, Lanzhou 730000, China

*Corresponding author: tian_miao@163.com

Phoxonic crystal is a periodic artificial structure that can manipulate optical and acoustic waves in the same temporal and spatial domain. It has broad application prospect in optical communication, optical mechanics sensor, quantum computations, phoxonic crystal integrated devices and so on. In this paper, we adopt a silicon-based two-dimensional square lattice structure, which can exhibit wide band gap of phonons and photons simultaneously. Then a periodic rectangular structure is introduced on the surface, the effects of the height and width of the rectangle on the optical and acoustic surface wave modes are analyzed. Based on the mode gap effect, a surface heterostructure composed of rectangles with different heights and widths is constructed. Then two identical surface heterostructures are placed face to face with an air slot in the middle, and connected with silicon substrate on both sides, which form an air slot heterostructure cavity. Five phononic cavity modes and three photonic cavity modes are obtained, the acousto-optical coupling rates between phononic and photonic cavity modes are calculated. The results show that the coupling rate between phononic and photonic cavity mode with the same symmetry and maximum overlap is the largest, and the coupling rates between the combination of phononic cavity modes α and β and photonic cavity modes can be adjusted by changing the phase difference φ of modes α and β. In this paper, the finite element method is used to simulate the calculation.

Keywords: phoxonic crystal, acousto-optic coupling, surface wave, air-slot.

1. Introduction

In recent years, phoxonic crystals have attracted more and more attention due to their properties of simultaneously manipulating light and sound waves at the same time [1]. Phoxonic crystals can serve as promising platform for enhancing the acousto-optic interaction in micro-and nano-structures [2-5]. They can be directly designed as acousto-optical dual-function device, such as waveguide [6-10], sensor [11-14], opti-

cal switch [15] *etc*., and they can also be used in quantum communication or quantum computing [16,17]. In 2006, Maldovan [18] proved theoretically for the first time that two-dimensional periodic structures can generate photonic and phononic band gaps at the same time. In 2009, Sadat-Saleh *et al*. [19] first proposed the concept of phoxonic crystals band gaps and discussed the influence of lattice form and structural geometric parameters on photonic and phononic band gaps in two-dimensional phoxonic crystals. That same year, Eichenfield *et al*. [20] proposed the concept of opto-mechanical crystal, and demonstrated the possibility of opto-mechanical crystal structure as a super-high precision force sensor through theoretical and experimental results. In 2010, Laude *et al*. [21] proposed a waveguide with perforated silicon nanostructures which can obtain wide phononic and photonic band gaps simultaneously. In 2012, Rolland *et al*. [22] studied acousto-optic coupling in periodic structures with simultaneous photonic and phononic bandgap based on the optical mechanical effect, which means the disturbance generated by acoustic mode affects the local optical mode in the cavity. In 2020, Shu *et al*. [23] studied the enhanced acousto-optic interaction in defect-free phoxonic waveguide, which use the abnormal dispersion properties in the passband instead of band gaps. In 2020, Ramp *et al*. [24] demonstrated that gallium arsenide in a three-dimensional microwave cavity can serve as a promising quantum state transduction platform, and their proposed opto-mechanical crystal structure has high sensitivity. In 2021, Afsari *et al*. [25] used a photonic crystal cavity model for hydrogen sulfide gas sensing and demonstrated that coating the surface of the cell with tungsten trioxide can improve the sensitivity of the sensor.

Two-dimensional phoxonic crystals with air slot structure have been studied by many researchers in recent years. Some studies have shown [26-32] that higher optical quality factors and higher acousto-optic coupling rates can be obtained by introducing air-slot structures. In 2010, Safavi-Naeini *et al*. [33] proposed a two-dimensional photonic crystal cavity model, with air slot structure, which has the advantage of higher optical quality factor. That same year, Jágerská *et al*. [34] proposed a photonic crystal sensor with an air cavity, and proved theoretically and experimentally that the air cavity structure has higher gas sensing sensitivity, which can be used for making a high sensitivity gas sensor with smaller volume. In 2015, Zhang *et al*. [35] proposed a model of a phoxonic crystal cavity with double air slots, which has small effective mass and higher optical quality factor. In 2017, Ma *et al*. [36] studied a two-dimensional phoxonic crystal structure with a slot, and theoretically proved that the structure with an air slot can effectively enhance the acousto-optic coupling effect. In 2020, Zhao *et al*. [37] proposed a dual channel photonic crystal with air slot, which proved theoretically and experimentally that the introduction of air slot is helpful to increase the optical quality factor.

In this paper, we adopt a silicon-based two-dimensional square lattice structure phoxonic crystal, which can exhibit wide band gap of phonons and photons simultaneously. Then, an air slot is introduced into the two-dimensional phoxonic crystal, and a rectangular periodic structure is added to the upper and lower surfaces of the air slot. The influences of the height and width of the rectangle on the surface wave dispersion

curves are analyzed. Then a heterostructure cavity with an air slot composed of rectangles with different heights and widths is constructed, in which several phononic and photonic cavity modes are localized and overlapped. Based on the moving boundary effect and the photoelastic effect, the acousto-optical coupling rates of different phononic and photonic cavity modes in the heterostructure cavity are calculated. The simulated data in this paper are calculated by the Finite Element Software COMSOL Multiphysics.

2. The design of heterostructure cavity with air slot

2.1. Band gap modulation of two-dimensional phoxonic crystals

Silicon based two-dimensional square lattice periodic structure with circular air holes is adopted to achieve wide phononic and photonic band gaps. Figure 1(a) is a schematic diagram of the crystal cell structure. Considering the application in the telecommunications field, the lattice constant of the structure is set as $a = 620$ nm, the radius of the circular air hole is r, and the first Brillouin zone of the lattice is shown in Fig. 1(b). The material used in the model is single crystal silicon, the basic optical and mechanical parameters are refractive index $n = 3.5$, mass density $\rho = 2331$ kg/m^3, elastic modulus $C_{11} = 16.57 \times 10^{10}$ N/m^2, $C_{12} = 6.39 \times 10^{10}$ N/m^2 [38]. The intrinsic frequencies of phonons and photons are measured as normalized frequencies (f_{c_t}/a) and (f_c/a) respectively, where c_t is the elastic shear wave velocity in silicon and c is the speed of light in air.

It is found that there are two bulk wave band gaps in the structure of phononic and photonic crystal, and the initial and cutoff frequency of the two bulk wave band gaps vary with the radius of the air hole. Figures 2(a) and (b) describe the curves of the initial and cut-off frequencies of the phononic and photonic band gaps with the air hole radius r, respectively. In Fig. 2(a), the width of the red and blue phononic band gaps in-
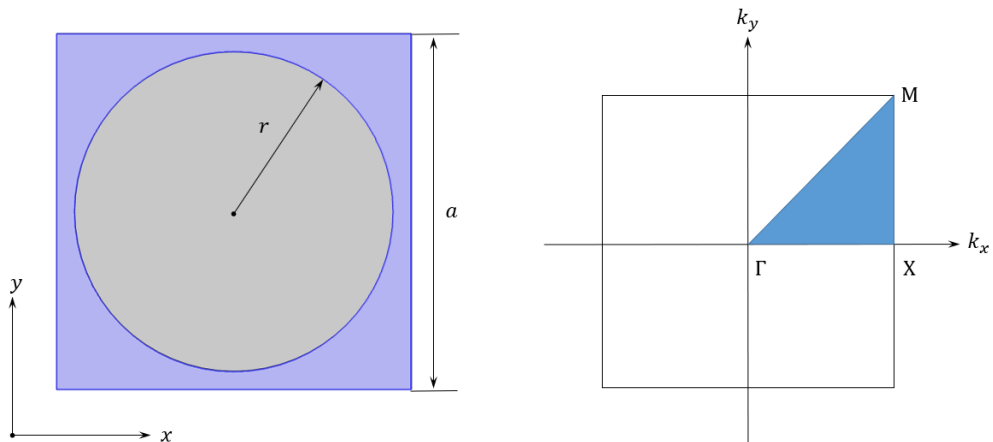

Fig. 1. (a) Primary cell diagram of the phoxonic crystal (air in gray and silicon substrate in blue); (b) the first Brillouin zone.
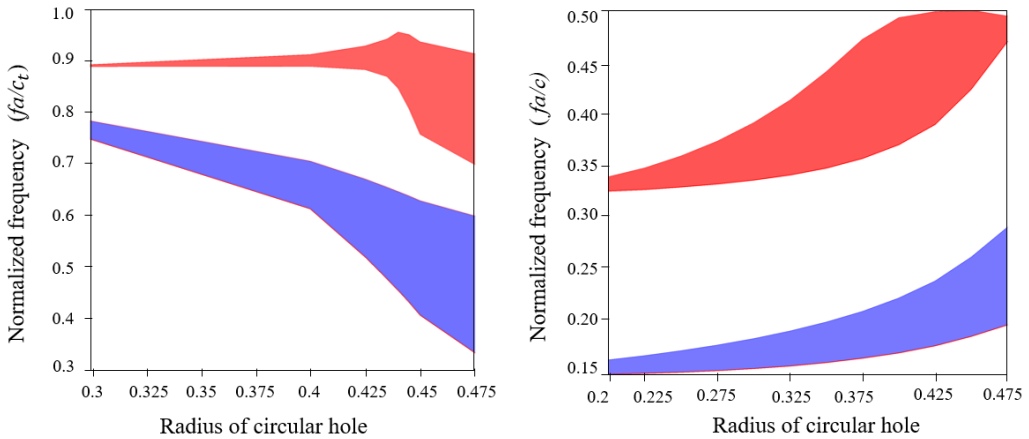
Fig. 2. (a) Phononic band gap initial and cutoff frequencies vary with the radius of the circular air holes; (b) photonic band gap initial and cutoff frequencies vary with the radius of the circular air holes. In (a) and (b), the blue part is the first band gap and the red part is the second band gap, the radius of the circular air holes is in unit of lattice constant a.

crease with the increase of the radius. In Fig. 2(b), the width of the blue photonic band gap increases with the increase of the radius, and the width of the red photonic band gap first increases and then decreases with the increase of the radius. Considering that the structure should have wider phononic and photonic band gap simultaneously, we choose the air hole radius $r = 0.45a$ as the parameter value of the subsequent design.

2.2. Surface structure design

Based on the two-dimensional phoxonic crystals introduced in the previous section, a row of cells is removed to form an air slot. A rectangular periodic structure is added on the upper and lower surfaces of the air slot. Figure 3(a) shows the supercell, which consists of 11 cells in the y direction with a defect in the centre, which is the air slot. Two identical rectangles are placed on the upper and lower surface of the air slot. The height and width of the rectangles are h and w respectively, and periodic boundary conditions are adopted on both sides of the supercell in the x direction. The phononic and photonic dispersion curves of the supercell structure are shown in Figs. 3(b) and (c) with the rectangle height $h = 0.25a$ and the width $w = 0.4a$. In Fig. 3(b), the gray region represents the phononic bulk wave band, and the two white regions are the phononic bulk wave band gaps. A surface phononic dispersion curve appears in the upper band gap, and three surface phononic dispersion curves appear in the lower band gap. On these curves, four points A, B, C and D are marked, the vibration modes corresponding to these points are shown in Fig. 3(d). In Fig. 3(c), the dark gray region is the photonic bulk band, the light gray region is the light cone, and the two white regions are the photonic band gaps. The corresponding electric field distribution modes in I and II are shown in Fig. 3(e). In Fig. 3(d), the modal distributions of four surface acoustic wave
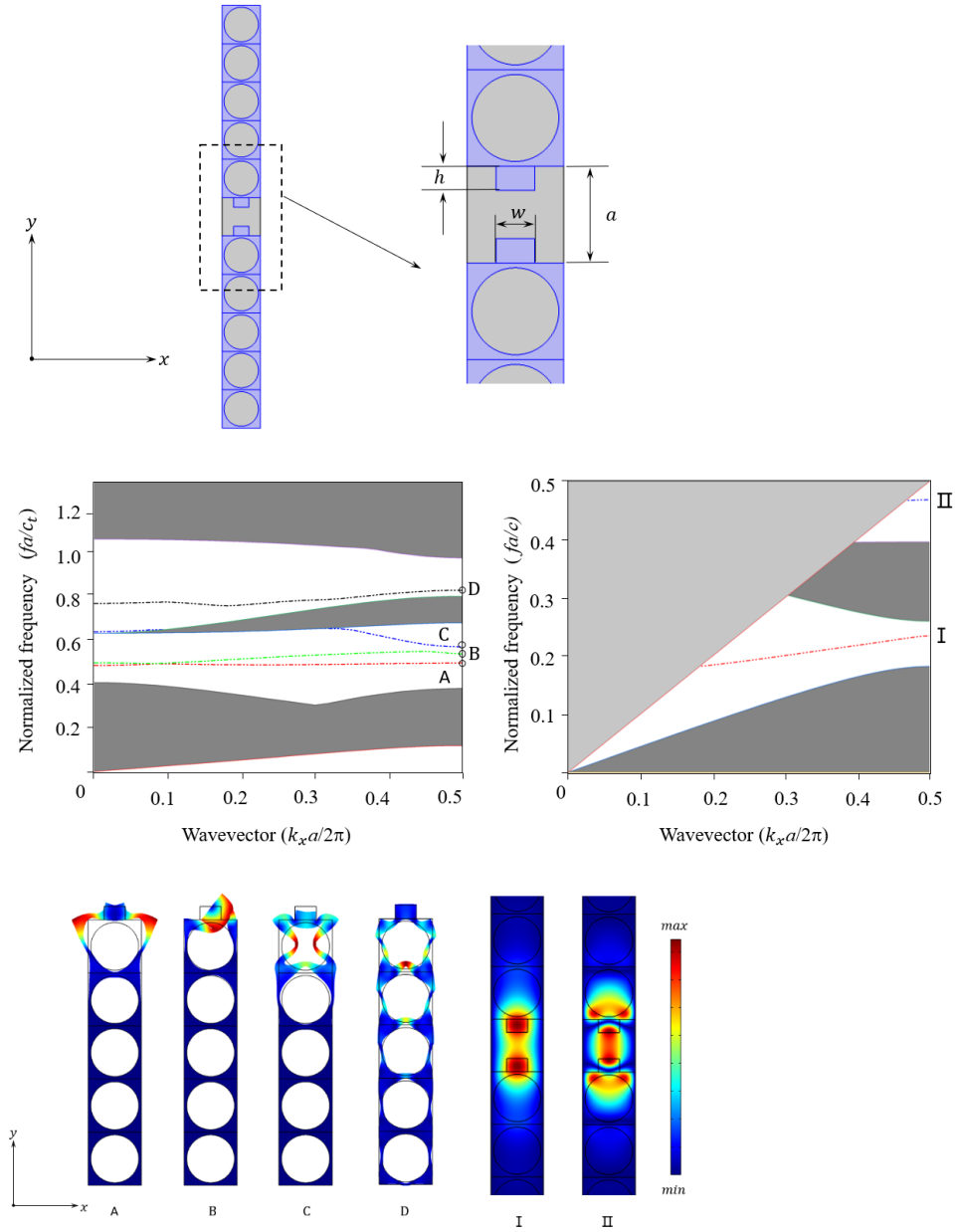
Fig. 3. (a) Phoxonic crystal supercell structure (the blue area is the silicon substrate and the gray area is air), *h* and *w* are the height and width of the rectangle, respectively. (b) Phononic dispersion curves with rectangle height $h = 0.25a$ and width $w = 0.4a$, the gray region represents the bulk wave energy band. (c) Photonic dispersion curves with rectangle height $h = 0.25a$ and width $w = 0.4a$, the dark gray region represents the bulk wave energy band, and the light gray region represents the light cone. (d) Vibration modes corresponding to points A, B, C and D; (e) Electric field distribution modes corresponding to I and II.

modes are shown, and the vibrations of these surface wave modes are mainly concentrated in the first layer of the substrate and the rectangle on the surface. The vibration of the A-point mode is mainly concentrated in the left and right upper parts of the air hole, and stretches to both sides along the x direction; this mode has an even parity in the x direction. The vibration of the B-point mode is concentrated in the surface rectangle, which is the torsion of the rectangle. The vibration of the C-point mode is concentrated on the left and right sides of the first layer of the matrix, and the left and right sides stretch toward the center of the circular hole; this mode has an even parity in the x direction. The vibration of the D-point mode concentrated on the first two layers of the matrix, stretched toward the center of the circular hole; this mode has even parity in the x direction. In Fig. 3(e), the electric field distribution of two surface optical wave modes were shown. Most of the energy of mode I is localized in the surface rectangular area, the eigenfrequency is 113.37 THz. The mode II energy is concentrated in three areas, namely the first layer of the silicon substrate in the middle, the surface rectangular area and the air slit area, and the eigenfrequency is 226.52 THz, approximately twice the eigenfrequency of mode I.

Next, we calculated the change rule of normalized frequency at the high symmetrical point X ($k_x a/2\pi = 0.5$) of the first Brillouin zone in the dispersion curve of acoustic surface wave and optical surface wave with the height h and width w of the rectangle, as shown in Fig. 4. Figure 4(a) describes the change rule of the normalized frequency of four surface acoustic waves corresponding to three different widths (red line represents $w = 0.3a$, green line represents $w = 0.35a$, and blue line represents $w = 0.4a$) with the height of the rectangle. These twelve curves can be divided into four sets in order of frequency from low to high, with three different colors forming a set. The first, second, and fourth sets of curves are all in the order of red, green and blue, while the third set of curves is in the reverse order of blue, green and red. As the height of the rectangle increases, the curves of the first and fourth sets remain basically horizontal, and the curves of the second and third set decrease slowly. Figure 4(b) depicts the change rule of normalized frequencies of four surface acoustic waves corresponding to three different heights (red line represents $h = 0.3a$, green line represents $h = 0.35a$, and blue line represents $h = 0.4a$) with the width of the rectangle. These twelve curves can also be divided into four sets in order of frequency from low to high, with three different colors forming a set. The four sets of curves are all in the order of red, green and blue. The three curves of the first set and the fourth set almost coincide. With the increase of the width of the rectangle, the second set of curves gradually rises, and the third set of curves gradually declines. From Fig. 4(a) and (b), it can be seen that the first and fourth surface acoustic waves are not sensitive to the height and width of the rectangle, the corresponding vibration modes of A and D in Fig. 3(d) show that the surface rectangle is almost undeformed. The second and third surface acoustic waves are less affected by the height of the rectangle, but more sensitive to the change of the width of the rectangle. Figure 4(c) shows how the normalized frequency of optical surface
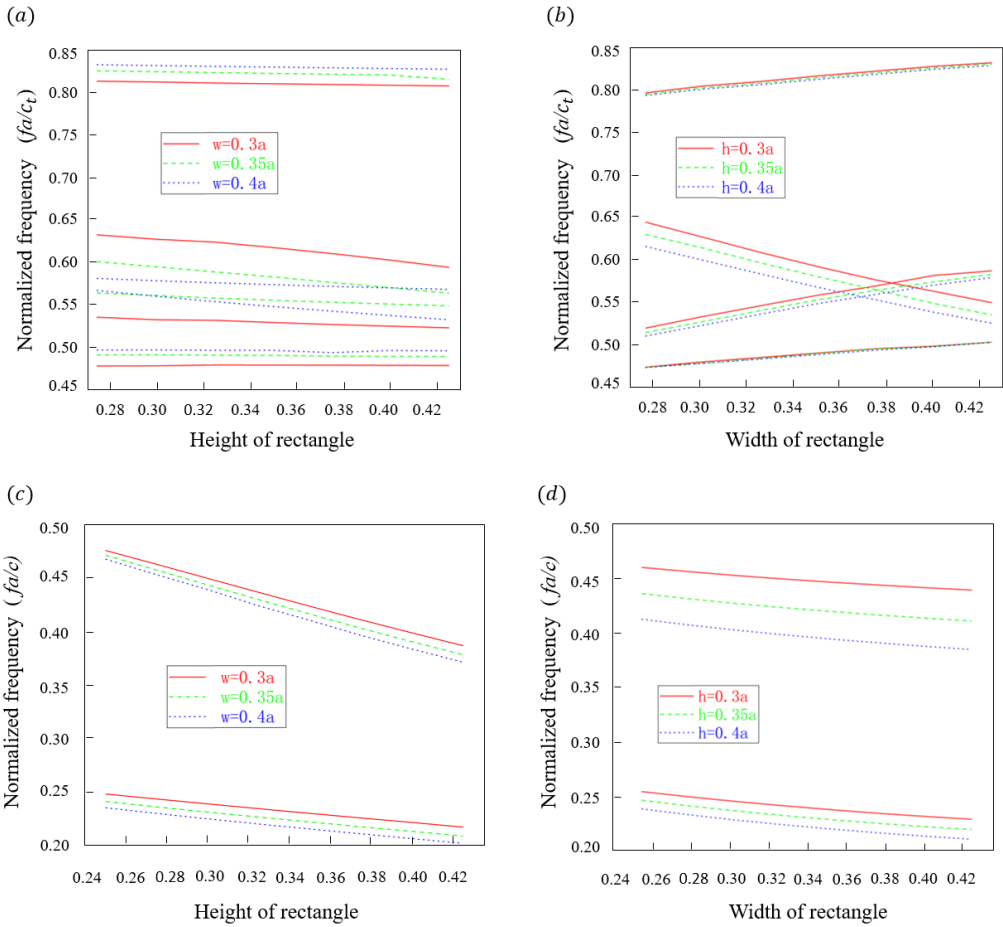
Fig. 4. (a) and (b) show the normalized frequency change at the point X of the acoustic surface dispersion curve with respect to the changes of the widths (heights) of the rectangle. (c) and (d) show the normalized frequency change at the point X of the optical surface dispersion curve with respect to the changes of the widths (heights) of the rectangle. (The height and width of the rectangle are in unit of lattice constant a.)

waves varies with the height of the rectangle at three different widths (the red line represents $w = 0.3a$, the green line represents $w = 0.35a$, and the blue line represents $w = 0.4a$). It can be seen that the normalized frequency of the two optical surface waves decreases with the increase of height. Figure 4(d) shows how the normalized frequency of optical surface waves varies with the width of the rectangle at three different heights (the red line represents $h = 0.3a$, the green line represents $h = 0.35a$, and the blue line represents $h = 0.4a$). It can be seen that the normalized frequency of the two optical surface waves decreases slowly as the rectangle width increases. Therefore, the optical surface wave is more sensitive to the change of the height of the rectangle. To sum up,

we can adjust the acoustic surface wave mode by setting different rectangle widths, and adjust the optical surface wave mode by setting different rectangle heights, and design the heterostructure cavity model based on this.

2.3. Design of heterostructure cavity

The design of the surface heterostructure cavity is based on the mode gap effect [39]. In the cavity region and barrier region of hetero-structure cavity, the structure parameters of surface rectangles are different, so there are mode gaps, which means some surface wave modes can be excited and exist in the cavity region, but cannot exist in the barrier region. Therefore, these modes are called the cavity modes. We selected two sets of rectangles with different parameters, namely parameter I: $h_1 = 0.25a$, $w_1 = 0.4a$ and parameter II: $h_2 = 0.4a$, $w_2 = 0.275a$. The corresponding surface wave dispersion curves are shown in Fig. 5. There are mode gaps between the phononic and photonic dispersion curves corresponding to these two sets of parameters, and the mode gap is indicated by yellow shadow in the figure.
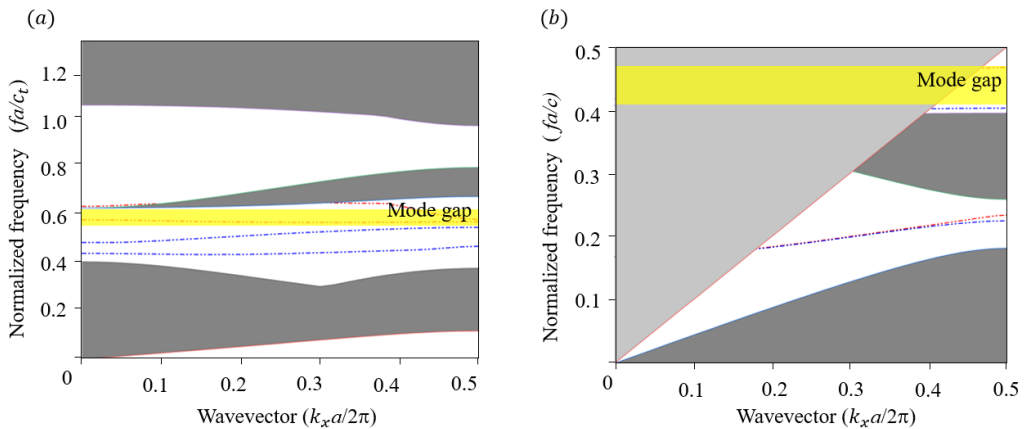

Fig. 5. Dispersion curves of surface acoustic wave (a) and optical surface wave (b) of phoxonic crystal. The red and blue lines are the results of $h_1 = 0.25a$, $w_1 = 0.4a$ and $h_2 = 0.4a$, $w_2 = 0.275a$, respectively. (The yellow shadows indicate the mode gaps.)

In the frequency range of the mode gap, there are surface modes in parameter I, but there is no surface mode in parameter II. Based on this, a hetero-structure cavity with air slot is designed, as shown in Fig. 6(a), the width of the cavity region is set as $4a$ with parameter I, and the width of the barrier area on both sides is set as $4a$ with parameter II. On both sides of the barrier region, two identical rectangular silicon with a width of a and a length of $11a$ are used to connect the upper and lower parts. There are five phononic cavity modes as shown in Fig. 6(b). Among them, the cavity mode α and β are equivalent but out of phase and both formed by the coupling of surface wave A and C modes with two C modes in the middle and A mode on both sides. The cavity mode γ is simply composed of surface wave B mode which has even parity
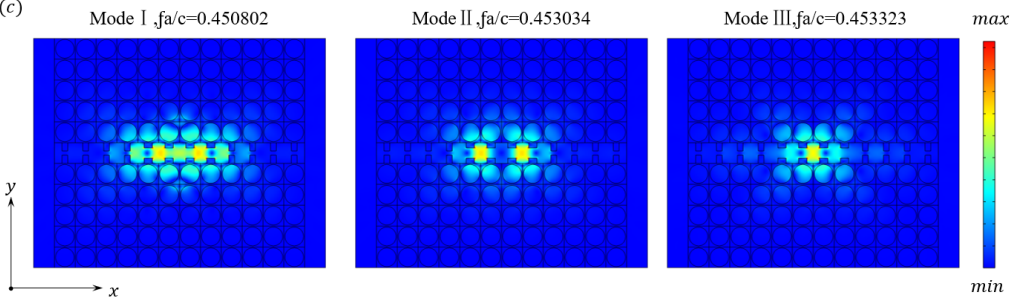
(*a*)
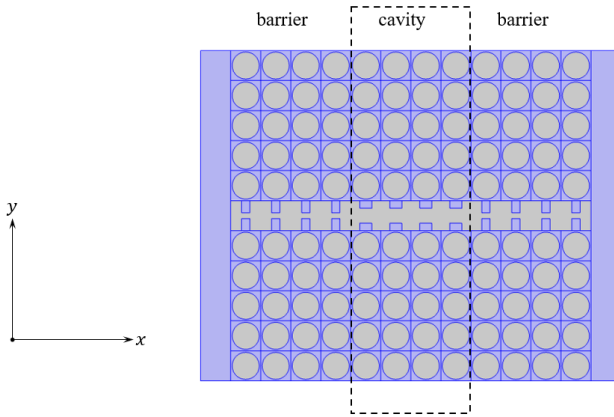
(*b*)
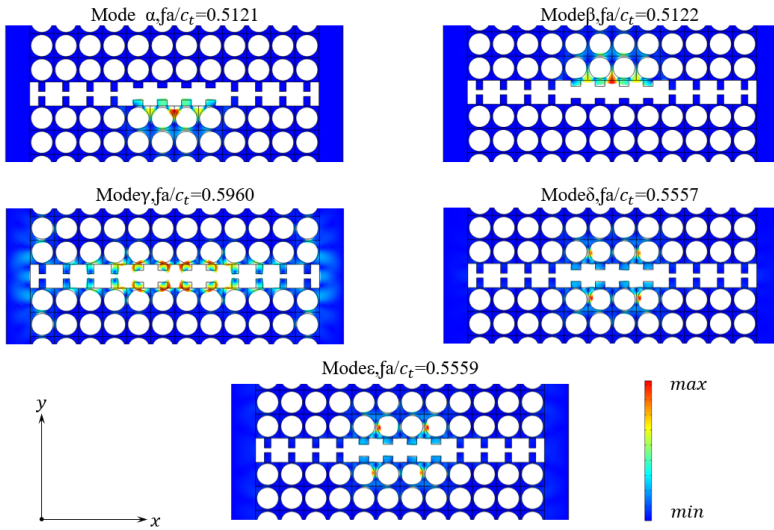
(*c*)

Fig. 6. (a) Two-dimensional phoxonic crystal heterostructure cavity with air slot. (b) Displacement field distribution of phononic cavity modes. (c) Electric field distribution of photonic cavity modes.

in the x and y directions. The cavity mode δ and ε are similar and both composed of the surface wave C mode, and the energy is mainly concentrated at the boundary between the two circles in the first layer of the upper and lower parts. For mode δ the vibrations in the upper and lower parts are going in the same direction, while for mode ε the vibrations are going in the opposite direction. Figure 6(c) depicts three photonic cavity modes with high quality factors, their optical vibrational energy is highly localized in the cavity region, and the electric field distribution has even parity in both x and y directions.

3. Acousto-optic coupling in heterostructure cavity

The strength of the acousto-optic coupling effect is measured by the acousto-optic coupling rate, it describes the frequency shift of the optical mode caused by the zero-point movement of the phonon cavity vibration, which is defined as

$$
g = \frac{\mathrm{d}\omega_0}{\mathrm{d}\alpha}\chi_{\mathrm{zpf}} = \frac{\mathrm{d}\omega_0}{\mathrm{d}\alpha}\sqrt{\frac{\hbar}{2m_{\mathrm{eff}}\,\omega_{\mathrm{m}}}} \tag{1}
$$

where ω_0 is the angular frequency of the optical field in the cavity, α is the generalized coordinate (amplitude of the displacement field in the cavity), χ_{zpf} is the amplitude of the zero-point motion of the acoustic resonator, m_{eff} is the effective moving mass of the phononic mode, and ω_{m} is the frequency of the acoustic mode. The physical meaning of acousto-optic coupling rate g can be understood as: when the amplitude of cavity vibration is χ_{zpf}, the frequency shift of the eigenfrequency of the optical mode is g.

According to the first-order electromagnetic perturbation theory, the contribution of the moving boundary effect to the acousto-optic coupling rate is

$$
g_{\mathrm{mb}} = -\frac{\omega_0}{2}\frac{\oint q\cdot\mathbf{n}(\Delta\varepsilon\,|E_{\|}|^2 - \Delta\varepsilon^{-1}|D_{\perp}|^2)\,\mathrm{d}A}{\int\varepsilon|E|^2\mathrm{d}V}\chi_{\mathrm{zpf}} \tag{2}
$$

where $\mathbf{n}$ is the outward normal of the cavity boundary, $E_{\|}$ represents the electric field component of the parallel interface, $D_{\perp}$ represents the electric displacement vector field component of the vertical interface, $\Delta\varepsilon = \varepsilon_{\mathrm{Si}} - \varepsilon_{\mathrm{air}}$ represents the variation of the permittivity, and $\Delta\varepsilon^{-1} = \varepsilon_{\mathrm{Si}}^{-1} - \varepsilon_{\mathrm{air}}^{-1}$ represents the variation of the reciprocal of the permittivity.

The contribution of the photoelastic effect to the acousto-optic coupling rate can be defined as

$$
g_{\mathrm{pe}} = -\frac{\omega_0}{2}\frac{\left\langle E\left|\dfrac{\mathrm{d}\varepsilon}{\mathrm{d}\alpha}\right|E\right\rangle}{\int\varepsilon|E|^2\mathrm{d}V}\chi_{\mathrm{zpf}} \tag{3}
$$

$$\langle E \left| \frac{\mathrm{d}\varepsilon}{\mathrm{d}\alpha} \right| E \rangle = -\varepsilon_0 n^4 \int \left\{ 2\operatorname{Re}\{E_x^* E_y\} p_{44} S_{xy} + 2\operatorname{Re}\{E_x^* E_z\} p_{44} S_{xz} \right.$$

$$+ 2\operatorname{Re}\{E_y^* E_z\} p_{44} S_{yz}$$

$$+ |E_x|^2 \left[p_{11} S_{xx} + p_{12}(S_{yy} + S_{zz}) \right]$$

$$+ |E_y|^2 \left[p_{11} S_{yy} + p_{12}(S_{xx} + S_{zz}) \right]$$

$$\left. + |E_z|^2 \left[p_{11} S_{zz} + p_{12}(S_{yy} + S_{xx}) \right] \right\} \mathrm{d}V \qquad (4)$$

where n is the refractive index of silicon, S_{kl} ($k, l = x, y$) is the elastic strain tensor, $p_{11} = -0.1$, $p_{12} = 0.01$, $p_{44} = -0.051$ are the photoelastic constant value. In the problem of acousto-optic coupling of phoxonic crystals, the acousto-optic coupling rate can be regarded as the sum of the contributions of the moving boundary effect and the photoelastic effect, and the total contribution of the acousto-optic coupling rate is

$$g = g_{\mathrm{mb}} + g_{\mathrm{pe}} \qquad (5)$$

The acousto-optic coupling strength in the phoxonic crystal structure can be calculated by referring to the above formula [40, 41].

Based on the above theoretical basis, we calculate the acousto-optic coupling rates corresponding to the five phononic cavity modes and three photonic cavity modes, which are shown in Table 1. Where the acousto-optic coupling rate is represented by g/χ_{zpf}, and its physical meaning is the frequency shift of the photonic cavity eigenfrequency in the unit vibration displacement.

It can be seen from Table 1 that the coupling rates between the three photonic cavity modes and the phononic cavity modes α and β are approximately equivalent in size but opposite in sign. The reason is that the vibration modes and eigenfrequency of the phononic cavity modes α and β are similar, but they have π phase difference. If the phononic cavity modes α and β are excited at the same time, denoted as $\alpha + \beta$ as shown in Fig. 7(a), the coupling rates will be greatly reduced due to mutual cancellation. But if the phononic cavity modes α and β are excited at the same time with phase difference φ, denoted as $\alpha + \beta\exp(i\varphi)$, the coupling rates can also be modulated by

T a b l e 1. The acousto-optic coupling rates between five phononic cavity modes and three photonic cavity modes (in units of THz·nm^{-1}).

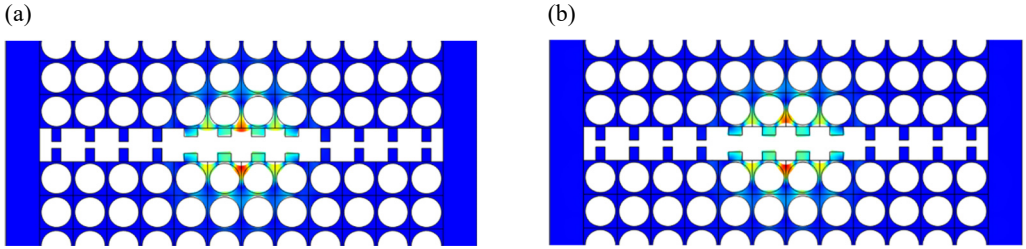|	Mode α	Mode β	Mode γ	Mode δ	Mode ε
I	-4.41×10^{-2}	4.47×10^{-2}	4.44×10^{-4}	6.42×10^{-5}	5.68×10^{-5}
II	-4.87×10^{-2}	4.94×10^{-2}	-8.63×10^{-2}	7.10×10^{-5}	1.28×10^{-4}
III	-6.15×10^{-2}	6.23×10^{-2}	3.13×10^{-2}	6.47×10^{-5}	-1.72×10^{-5}

(a)

(b)

Fig. 7. (a) Modes α and β are excited at the same time, denoted as $\alpha + \beta$. (b) Modes α and β are excited at the same time with the phase difference π, denoted as $\alpha - \beta$.

(a) mode $\alpha + \beta$ and photonic cavity mode II

(b) mode $\alpha - \beta$ and photonic cavity mode II

(c) mode $\alpha + \beta$ and photonic cavity mode III
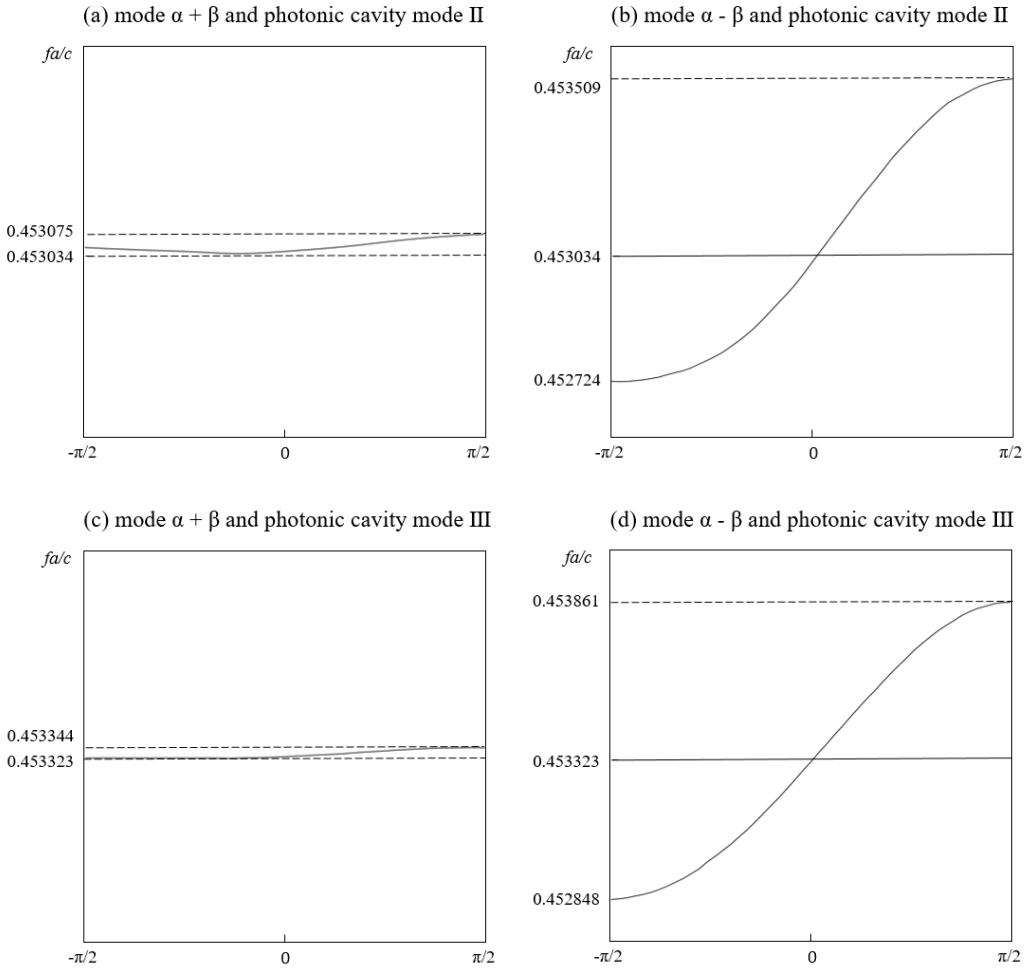
(d) mode $\alpha - \beta$ and photonic cavity mode III

Fig. 8. Modulations of the photonic cavity modes II and III frequencies by the acoustic mode $\alpha + \beta$ and $\alpha - \beta$.

changing the phase difference φ. When the phase difference $\varphi = \pi$, and $\alpha + \beta\exp(i\varphi) =$ $= \alpha + \beta\exp(i\pi) = \alpha - \beta$ as shown in Fig. 7(b).

The quasi-static method is used to illustrate the acousto-optical coupling. The frequency of light waves is several orders of magnitude higher than that of elastic waves. Compared with light waves, the vibration of elastic wave is very slow, which means quasi static. If the half cycle of an elastic wave is divided into 50 equal parts, there are 51 moments. At each moment, the frequency of optical modes generated by deformed cavity can be calculated. Thus, the change in the frequency of the optical cavity mode within half an elastic wave period can be obtained. The modulations of the photonic cavity modes II and III frequencies by the acoustic modes $\alpha + \beta$ and $\alpha - \beta$ are shown in Fig. 8, which indicate the mode $\alpha - \beta$ has a greater coupling rates.

The coupling rates between the three photonic cavity modes and the phononic cavity modes δ and ε are small, the reason is that the vibrations of the phononic cavity modes δ and ε are mainly concentrated at the connection between the circular holes in the first layer, and there is almost no vibration on the surface rectangles. The overlap between the phononic cavity mode and the photonic cavity mode is low. The coupling rate between photonic cavity mode II and phononic cavity mode γ is the highest, and the eigenfrequency of photonic cavity mode II is 219.21 THz, and the optical quality factor is 16645.66. Table 2 lists the contributions of the moving boundary effect and the photoelastic effect to the coupling rate of the photonic cavity mode II and the

T a b l e 2. Acousto-optic coupling rates of phononic cavity mode γ and photonic cavity mode II (in units of THz·nm^{-1}).

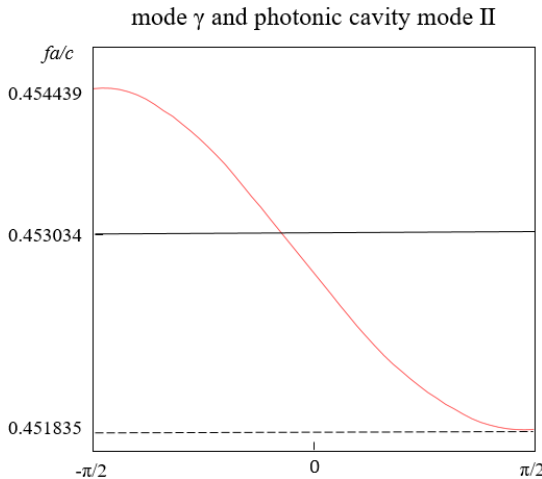|	g_{mb}/χ_{zpf}	g_{pe}/χ_{zpf}	g/χ_{zpf}
Mode γ	-4.30×10^{-2}	-4.34×10^{-2}	-8.63×10^{-2}

Fig. 9. Modulations of the photonic cavity mode II frequency by the acoustic mode γ.

phononic cavity mode γ respectively, and the contributions of the two effects to the coupling rate are equivalent. The modulations of the photonic cavity mode II frequency by the acoustic modes γ can also be calculated by using quasi-static method, as shown in Fig. 9.

The vibration energy of the phononic cavity mode γ is mainly concentrated on the surface rectangle of the cavity region, and the vibration mode is the torsion of the rectangle, with even parity in both x and y directions. The photonic cavity mode II and the phononic cavity mode γ have the largest overlap degree and the same symmetry, so they have the largest acousto-optical coupling rate, where the torsional tensile deformation of the surface rectangle leads to a large photoelastic effect, while the change of the surface shape is what causes the moving boundary effect.

4. Conclusion

In this paper, we adopt a silicon-based two-dimensional square lattice structure, which can exhibit wide band gap of phonons and photons simultaneously. Then a periodic rectangular structure is introduced on the surface, the effects of the height and width of the rectangle on the optical and acoustic surface wave modes are analyzed. The phononic surface mode can be well adjusted by changing the rectangle width, and the photonic surface mode can be well adjusted by changing the rectangle height. Based on mode gap theory, a heterostructure cavity with air-slot is proposed. Then five phononic cavity modes and three photonic cavity modes are obtained. The coupling rates between these phononic cavity modes and photonic cavity modes were calculated based on the moving boundary effect and the photoelastic effect. The results show that the phononic cavity mode γ and photonic cavity mode II have the highest coupling rate, and the coupling rates between the combination of modes α and β and the photonic cavity modes can be adjusted by changing the phase difference φ between the modes α and β.

References

[1] Pennec Y., Laude V., Papanikolaou N., Djafari-Rouhani B., Oudich M., Jallal S.E., Beugnot J.C., Escalante J.M., Martínez A., *Modeling light-sound interaction in nanoscale cavities and waveguides*, Nanophotonics **3**, 2014: 413-440. https://doi.org/10.1515/nanoph-2014-0004
[2] Hassouani Y.E., Li C., Pennec Y., El Boudouti E.H., Larabi H., Akjouj A., Matar O.B., Laude V., Papanikolaou N., Martinez A., Rouhani B.D., *Dual phononic and photonic band gaps in a periodic array of pillars deposited on a thin plate*, Physical Review B **82**, 2010: 155405. https://doi.org/10.1103/PhysRevB.82.155405

[3] BRIA M., ASSOUAR B., OUDICH M., PENNEC Y., VASSEUR J., DJAFARI-ROUHANI B., *Opening of simultaneous photonic and phononic band gap in two-dimensional square lattice periodic structure*, Journal of Applied Physics **109**, 2011: 014507. https://doi.org/10.1063/1.3530682

[4] ROLLAND Q., DUPONT S., GAZALET J., KASTELIK J., PENNEC Y., DJAFARI-ROUHANI B., LAUDE V., *Simultaneous bandgaps in LiNbO$_3$ phoxonic crystal slab*, Optics Express **22**, 2014: 16288-16297. https://doi.org/10.1364/OE.22.016288

[5] PAPANIKOLAOU N., PSAROBAS I.E., STEFANOU N., *Absolute spectral gaps for infrared light and hypersound in three-dimensional metallodielectric phoxonic crystals*, Applied Physics Letters **96**, 2010: 231917. https://doi.org/10.1063/1.3453448

[6] HSIAO F., HSIEH C., HSIEH H., CHIU C., *High-efficiency acousto-optical interaction in phoxonic nanobeam waveguide*, Applied Physics Letters **100**, 2012: 171103. https://doi.org/10.1063/1.4705295

[7] ARAM M.H., KHORASANI S., *Optical wave evolution due to interaction with elastic wave in a phoxonic crystal slab waveguide*, Applied Physics B **123**, 2017: 1-9. https://doi.org/10.1007/s00340-017-6792-x

[8] PENNEC Y., ROUHANI B.D., LI C., ESCALANTE J.M., MARTINEZ A., BENCHABANE S., LAUDE V., PAPANIKOLAOU N., *Band gaps and cavity modes in dual phononic and photonic strip waveguides*, AIP Advances **1**, 2011: 041901. https://doi.org/10.1063/1.3675799

[9] LIU K., YUAN X.D., YE W.M., ZENG C., *Air waveguide in a hybrid 1D and 2D photonic crystal heterostructure*, Optics Communications **282**, 2009: 4445-4448. https://doi.org/10.1016/j.optcom.2009.08.001

[10] ELSHAHAT S., ABOOD I., LIANG Z.X., PEI J.H., OUYANG Z.B., *Sporadic-slot photonic-crystal waveguide for all-optical buffers with low-dispersion, distortion, and insertion loss*, IEEE Access **8**, 2020: 77689-77700. https://doi.org/10.1109/ACCESS.2020.2986082

[11] PENNEC Y., JIN Y., ROUHANI B.D., *Phononic and photonic crystals for sensing applications*, Advances in Applied Mechanics **52**, 2019: 105-145. https://doi.org/10.1016/bs.aams.2018.11.001

[12] FORZANI L., MENDEZ C.G., URTEAGA R., HUESPE A.E., *Design and optimization of an opto-acoustic sensor based on porous silicon phoxonic crystals*, Sensors and Actuators A **331**, 2021: 112915. https://doi.org/10.1016/j.sna.2021.112915

[13] TAYOUB H., HOCINI A., HARHOUZ A., *High-sensitive mid-infrared photonic crystal sensor using slotted-waveguide coupled-cavity*, Progress In Electromagnetics Research M **105**, 2021: 45-54. http://dspace.univ-msila.dz:8080//xmlui/handle/123456789/30220

[14] HOANG T.H.C., *Analysis on slotted photonic crystal cavity and waveguide combination in silicon-on-insulator platform*, Optik **251**, 2022: 168465. https://doi.org/10.1016/j.ijleo.2021.168465

[15] CHEN G.D., ZHANG R., SUN J., *On-chip optical mode conversion based on dynamic grating in photonic-phononic hybrid waveguide*, Scientific Reports **5**, 2015: 1-7. https://doi.org/10.1038/srep10346

[16] TEUFEL J.D., LI D., ALLMAN M.S., CICAK K., SIROIS A.J., WHITTAKER J.D., SIMMONDS R.W., *Circuit cavity electromechanics in the strong-coupling regime*, Nature **471**(7337), 2011: 204-208. https://doi.org/10.1038/nature09898

[17] GROBLACHER S., HAMMERER K., VANNER M.R., ASPELMEYER M., *Observation of strong coupling between a micromechanical resonator and an optical cavity field*, Nature **460**(7256), 2009: 724-727. https://doi.org/10.1038/nature08171

[18] MALDOVAN M., THOMAS E.L., *Simultaneous localization of photons and phonons in two-dimensional periodic structures*, Applied Physics Letters **88**, 2006: 251907. https://doi.org/10.1063/1.2216885

[19] SADAT-SALEH S., BENCHABANE S., BAIDA F.I., BERNAL M., LAUDE V., *Tailoring simultaneous photonic and phononic band gaps*, Journal of Applied Physics **106**, 2009: 074912. https://doi.org/10.1063/1.3243276

[20] EICHENFIELD M., CHAN J., CAMACHO R.M., VAHALA K.J., PAINTER O., *Optomechanical crystals*, Nature **462**, 2009: 78-82. https://doi.org/10.1038/nature08524

[21] LAUDE V., BEUGNOT J.-C., BENCHABANE S., PENNEC Y., DJAFARI-ROUHANI B., PAPANIKOLAOU N., MARTINEZ A., *Design of waveguides in silicon phoxonic crystal slabs*, [In] *2010 IEEE International Ultrasonics Symposium*, San Diego, CA, USA, October 11-14, 2010. https://doi.org/10.1109/ULTSYM.2010.5935703

[22] Rolland Q., Oudich M., El-Jallal S., Dupont S., Pennec Y., Gazalet J., Kastelik J.C., Lévêque G., Djafari-Rouhani B., *Acousto-optic couplings in two-dimensional phoxonic crystal cavities*, Applied Physics Letters **101**, 2012: 061109. https://doi.org/10.1063/1.4744539

[23] Shu Y.Y., Yu M.H., Yu T.B., Liu W.X., Wang T.B., Liao Q.H., *Design of phoxonic virtual wave-guides for both electromagnetic and elastic waves based on the self-collimation effect: an application to enhance acousto-optic interaction*, Optics Express **28**(17), 2020: 24813-24819. https://doi.org/10.1364/OE.399591

[24] Ramp H., Clark T.J., Hauer B.D., Doolin C., Balram K.C., Srinivasan K., Davis J.P., *Wavelength transduction from a 3D microwave cavity to telecom using piezoelectric optomechanical crystals*, Applied Physics Letters **116**, 2020: 174005. https://doi.org/10.1063/5.0002160

[25] Afsari A., Sarraf M.J., Khatib F., *Application of tungsten oxide thin film in the photonic crystal cavity for hydrogen sulfide gas sensing*, Optik **227**, 2021: 165664. https://doi.org/10.1016/j.ijleo.2020.165664

[26] Mosbah C., Benmerkhi A., Bouchemat M., Bouchemat T., *Design of refractive index sensing based on 2D PhC air-slot width-modulated line-defect microcavity*, Optical and Quantum Electronics **51**, 2019: 1-14. https://doi.org/10.1007/s11082-019-1871-3

[27] Wang C., Quan Q., Kita S., Li Y., Lončar M., *Single-nanoparticle detection with slot-mode photonic crystal cavities*, Applied Physics Letters **106**, 2015: 261105. https://doi.org/10.1063/1.4923322

[28] Almeida V.R., Xu Q., Barrios C.A., Lipson M., *Guiding and confining light in void nanostructure*, Optics Letters **29**, 2004: 1209-1211. https://doi.org/10.1364/OL.29.001209

[29] Robinson J.T., Manolatou C., Chen L., Lipson M., *Ultrasmall mode volumes in dielectric optical micro-cavities*, Physical Review Letters **95**, 2005: 143901. https://doi.org/10.1103/PhysRevLett.95.143901

[30] Di Falco A., O'Faolain L., Krauss T.F., *Chemical sensing in slotted photonic crystal heterostruc-ture cavities*, Applied Physics Letters **94**(6), 2009: 063503. https://doi.org/10.1063/1.3079671

[31] Ryckman J.D., Sharon M.W., *Localized field enhancements in guided and defect modes of a pe-riodic slot waveguide*, IEEE Photonics Journal **3**, 2011: 986-995. https://doi.org/10.1109/JPHOT.2011.2170966

[32] Gao J., McMillan J.F., Wu M.C., Zheng J., Assefa S., Wong C.W., *Demonstration of an air-slot mode-gap confined photonic crystal slab nanocavity with ultrasmall mode volumes*, Applied Phys-ics Letters **96**, 2010: 051123. https://doi.org/10.1063/1.3298642

[33] Safavi-Naeini A.H., Alegre T.P.M., Winger M., Painter O., *Optomechanics in an ultrahigh-Q two-dimensional photonic crystal cavity*, Applied Physics Letters **97**, 2010: 181106. https://doi.org/10.1063/1.3507288

[34] Jágerská J., Zhang H., Diao Z., Thomas N.L., Houdré R., *Refractive index sensing with an air-slot photonic crystal nanocavity*, Optics Letters **35**, 2010: 2523-2525. https://doi.org/10.1364/OL.35.002523

[35] Zhang H., Zhang Y., Gao G., Zhao X., Wang Y., Huang Q., Xia J., *Design of a femtogram scale double-slot photonic crystal optomechanical cavity*, Optics Express **23**, 2015: 23167-23176. https://doi.org/10.1364/OL.35.002523

[36] Ma T.X., Wang Y.S., Zhang C., *Enhancement of acousto-optical coupling in two-dimensional air -slot phoxonic crystal cavities by utilizing surface acoustic waves*, Physics Letters A **381**, 2017: 323-329. https://doi.org/10.1016/j.physleta.2016.10.052

[37] Zhao Y.X., Buchholz J.H., Grenter T., Liu X., Bögel G.V., Seidl K., Balzer J.C., *Sensitive and robust millimeter-wave/terahertz photonic crystal chip for biosensing applications*, IEEE Access **10**, 2022: 92237-92248. https://doi.org/10.1109/ACCESS.2022.3202537

[38] Chan J., Safavi-Naeini A.H., Hill J.T., Meenehan S., Painter O., *Optimized optomechanical crys-tal cavity with acoustic radiation shield*, Applied Physics Letters **101**, 2012: 081115. https://doi.org/10.1063/1.4747726

[39] Song B.S., Noda S., Asano T., Akahane Y., *Ultra-high-q photonic double-heterostructure nano-cavity*, Nature Materials **4**, 2005: 207-210. https://doi.org/10.1038/nmat1320

[40] LI Y.Z., CUI K., FENG X., HUANG Y., HUANG Z., LIU F., ZHANG W., *Optomechanical crystal nanobeam cavity with high optomechanical coupling rate*, Journal of Optics **17**, 2015: 045001. https://doi.org/10.1088/2040-8978/17/4/045001

[41] GAVARTIN E., BRAIVE R., SAGNES I., ARCIZET O., BEVERATOS A., KIPPENBERG T.J., ROBERT-PHILIP I., *Optomechanical coupling in a two-dimensional photonic crystal defect cavity*, Physical Review Letters **106**, 2011: 203902. https://doi.org/10.1103/PhysRevLett.106.203902